Electronic Supplementary Material (ESI) for Dalton Transactions.

- Supporting Information –

Comparing London Dispersion Pnictogen-π Interactions in Naphthyl-substituted Dipnictanes

Alexander Gehlhaar,[a] Eduardo Schiavo,[b] Christoph Wölper,[a] Yannick Schulte,[a] Alexander A. Auer,[b]* Stephan Schulz[a]*

[a.] *Institute for Inorganic Chemistry and Center for Nanointegration Duisburg-Essen (Cenide), University of Duisburg-Essen, Universitätsstraße 5-7, D-45117 Essen, Germany.*

[b.] *Max-Planck-Institut für Kohlenforschung, D-45470 Mülheim an der Ruhr, Germany*

Table of Contents:

A) Experimental Details

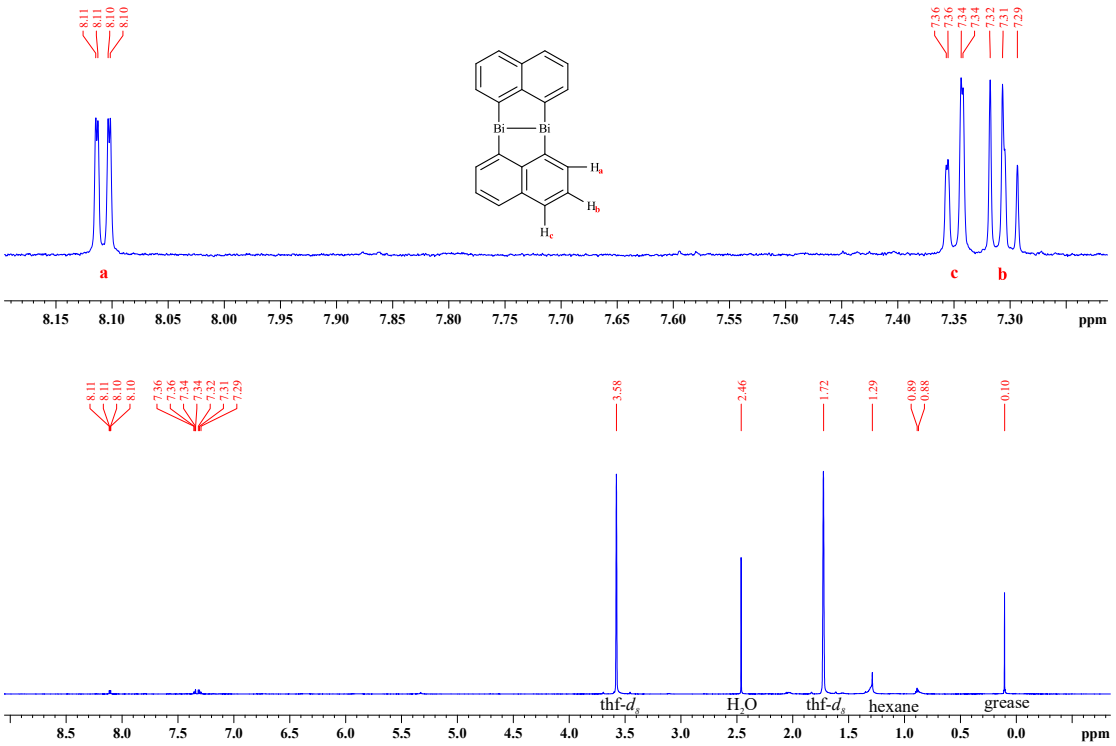

Figure S1. ^{1}H NMR spectrum of **1** in thf-d_8. Due to the low solubility of **1** impurities appear more prominent.

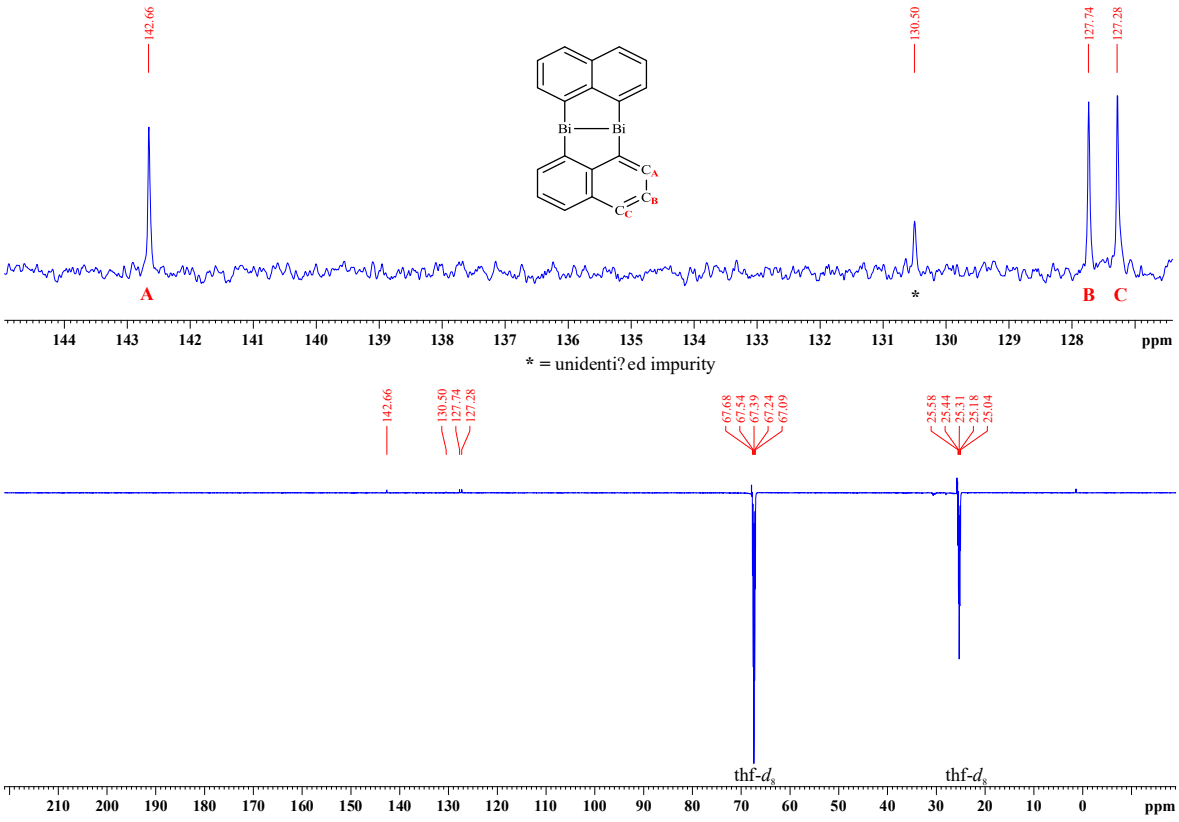

Figure S2. DEPTQ-135 ^{13}C{^{1}H} NMR spectrum of **1** in thf-d_8. Due to the low solubility of **1** impurities appear more prominent and quaternary carbons could not be observed.

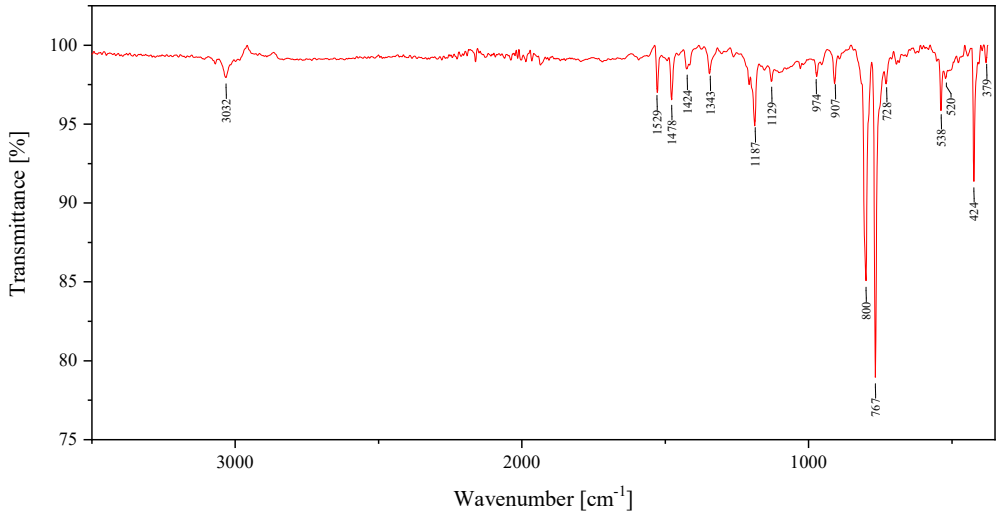

Figure S3. IR spectrum of neat **1**.

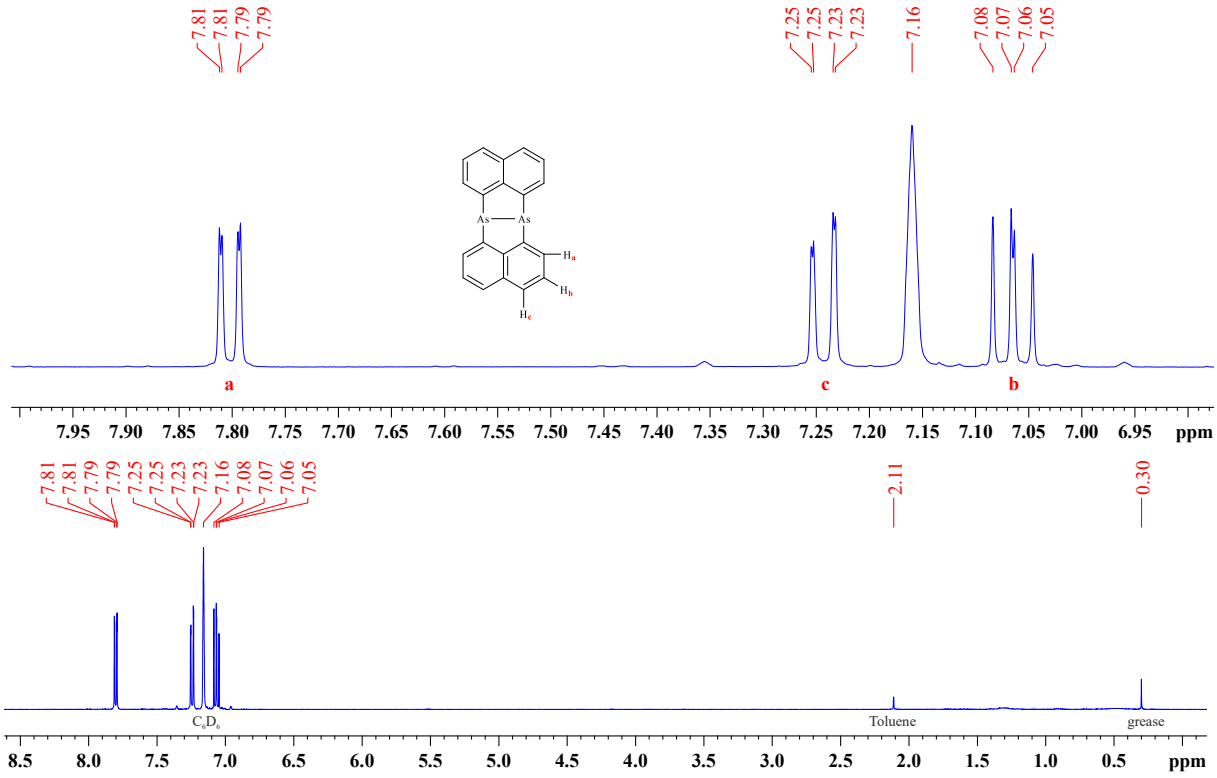

Figure S4. ^{1}H NMR spectrum of **2** in C_6D_6.

B) Crystallographic Details

Table S3. Single crystal X-ray diffraction data of **1** and **2**.

Compound	**1**	**2**
Empirical formula	$C_{20}H_{12}Bi_2$	$C_{20}H_{12}As_2$
M	670.26	402.14
Crystal size [mm]	0.124 × 0.045 × 0.031	0.177 × 0.069 × 0.067
T [K]	100(2)	100(2)
Crystal system	monoclinic	triclinic
Space group	$C2/c$	P-1
a [Å]	19.3995(17)	8.3154(8)
b [Å]	5.1523(4)	9.7984(10)
c [Å]	31.532(3)	10.2317(7)
α [°]	90	75.105(6)
β [°]	98.603(4)	69.115(6)
γ [°]	90	78.997(8)
V [Å^3]	3116.2(5)	748.15(12)
Z	8	2
D_{calc} [g·cm^{-3}]	2.857	1.785
μ(MoK_α [mm^{-1}])	22.550	5.450
Transmissions	0.02/0.01	0.75/0.57
F(000)	2384	396
Index ranges	$-25 \le h \le 25$	$-10 \le h \le 9$
	$-6 \le k \le 6$	$-12 \le k \le 12$
	$-41 \le l \le 41$	$-13 \le l \le 13$
ϑ_{max} [°]	28.329	80.944
Reflections collected	17944	65245
Independent reflections	3860	3269
R_{int}	0.1025	0.0385
Refined parameters	199	199
R_1 [$I > 2\sigma(I)$]	0.0550	0.0260
wR_2 [all data]	0.1109	0.0690
GooF	1.006	1.061
$\Delta\rho_{final}$ (max/min) [e·Å^{-3}]	1.812/-1.382	1.685/-0.847
Empirical formula	$C_{20}H_{12}Bi_2$	$C_{20}H_{12}As_2$

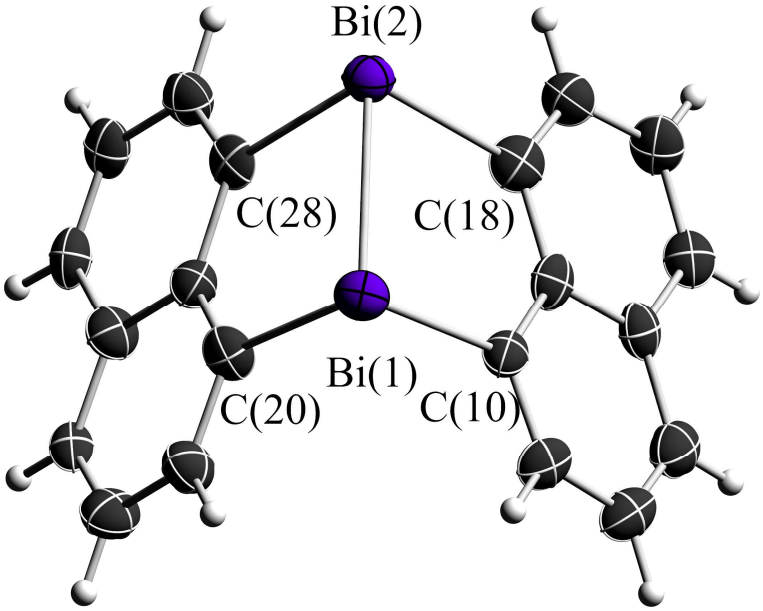

Figure S5. Solid state structure of **1**. Displacement ellipsoids drawn at 50 % probability levels.

Table S4. Bond lengths [Å] of **1**.

Bi1-C10	2.241(13)	C17-C18	1.36(2)
Bi1-C20	2.271(15)	C18-C19	1.42(2)
Bi1-Bi2	2.8964(8)	C20-C21	1.391(19)
Bi2-C28	2.249(14)	C20-C29	1.400(19)
Bi2-C18	2.264(16)	C21-C22	1.41(2)
C10-C11	1.331(18)	C22-C23	1.39(2)
C10-C19	1.440(19)	C23-C24	1.386(18)
C11-C12	1.40(2)	C24-C29	1.449(19)
C12-C13	1.36(2)	C24-C25	1.46(2)
C13-C14	1.42(2)	C25-C26	1.324(19)
C14-C15	1.427(18)	C26-C27	1.40(2)
C14-C19	1.44(2)	C27-C28	1.363(19)
C15-C16	1.36(2)	C28-C29	1.477(18)
C16-C17	1.41(2)		

Table S5. Bond angles [°] of **1**.

C10-Bi1-C20	89.1(5)	C18-C19-C10	124.0(13)
C10-Bi1-Bi2	85.2(3)	C18-C19-C14	117.7(13)
C20-Bi1-Bi2	84.7(3)	C10-C19-C14	118.3(12)
C28-Bi2-C18	92.2(5)	C21-C20-C29	120.0(14)
C28-Bi2-Bi1	85.9(3)	C21-C20-Bi1	115.7(11)
C18-Bi2-Bi1	85.4(4)	C29-C20-Bi1	124.1(10)
C11-C10-C19	117.9(13)	C20-C21-C22	120.2(15)
C11-C10-Bi1	118.9(11)	C23-C22-C21	121.3(14)
C19-C10-Bi1	123.1(9)	C22-C23-C24	119.0(13)
C10-C11-C12	125.1(14)	C23-C24-C29	120.8(13)
C13-C12-C11	119.5(15)	C23-C24-C25	121.4(12)
C12-C13-C14	119.4(15)	C29-C24-C25	117.7(13)
C13-C14-C15	121.3(14)	C26-C25-C24	120.3(13)
C13-C14-C19	119.9(13)	C25-C26-C27	123.2(14)
C15-C14-C19	118.8(13)	C28-C27-C26	121.2(13)
C16-C15-C14	121.9(14)	C27-C28-C29	119.2(13)
C15-C16-C17	118.4(13)	C27-C28-Bi2	118.8(10)
C18-C17-C16	122.8(14)	C29-C28-Bi2	122.0(10)
C17-C18-C19	120.4(15)	C20-C29-C24	118.7(13)
C17-C18-Bi2	117.5(12)	C20-C29-C28	123.0(13)
C19-C18-Bi2	122.1(11)	C24-C29-C28	118.3(12)

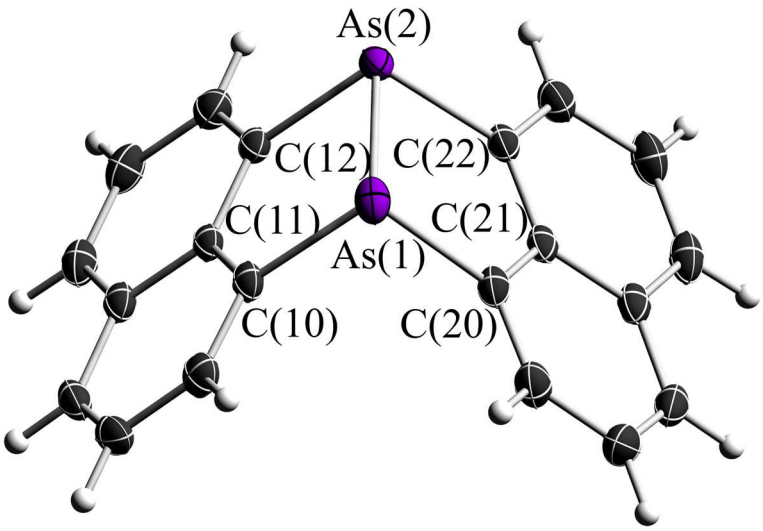

Figure S6. Solid state structure of **2**. Displacement ellipsoids drawn at 50 % probability levels.

Table S4. Bond lengths [Å] of **2**.

As1-C10	1.963(2)	C17-C18	1.370(3)
As1-C20	1.965(2)	C18-C19	1.408(3)
As1-As2	2.4471(4)	C20-C29	1.372(3)
As2-C22	1.964(2)	C20-C21	1.420(3)
As2-C12	1.966(2)	C21-C22	1.419(3)
C10-C19	1.375(3)	C21-C26	1.430(3)
C10-C11	1.422(3)	C22-C23	1.377(3)
C11-C16	1.423(3)	C23-C24	1.412(3)
C11-C12	1.425(3)	C24-C25	1.366(4)
C12-C13	1.377(3)	C25-C26	1.416(3)
C13-C14	1.408(3)	C26-C27	1.418(3)
C14-C15	1.365(3)	C27-C28	1.366(4)
C15-C16	1.421(3)	C28-C29	1.410(3)
C16-C17	1.422(3)		

Table S5. Bond angles [°] of **2**.

C10-As1-C20	96.09(8)	C18-C17-C16	120.6(2)
C10-As1-As2	90.87(6)	C17-C18-C19	120.4(2)
C20-As1-As2	90.54(6)	C10-C19-C18	120.6(2)
C22-As2-C12	97.62(8)	C29-C20-C21	120.2(2)
C22-As2-As1	90.26(6)	C29-C20-As1	121.13(17)
C12-As2-As1	90.17(6)	C21-C20-As1	118.60(15)
C19-C10-C11	120.28(19)	C22-C21-C20	121.51(19)
C19-C10-As1	121.22(16)	C22-C21-C26	119.43(19)
C11-C10-As1	118.49(15)	C20-C21-C26	119.05(19)
C10-C11-C16	119.09(18)	C23-C22-C21	120.1(2)
C10-C11-C12	121.42(18)	C23-C22-As2	120.94(17)
C16-C11-C12	119.49(19)	C21-C22-As2	118.92(15)
C13-C12-C11	119.81(19)	C22-C23-C24	120.1(2)
C13-C12-As2	121.17(16)	C25-C24-C23	121.1(2)
C11-C12-As2	119.01(15)	C24-C25-C26	120.5(2)
C12-C13-C14	120.5(2)	C25-C26-C27	122.3(2)
C15-C14-C13	120.9(2)	C25-C26-C21	118.7(2)
C14-C15-C16	120.5(2)	C27-C26-C21	118.9(2)
C15-C16-C17	122.3(2)	C28-C27-C26	120.4(2)
C15-C16-C11	118.8(2)	C27-C28-C29	120.8(2)
C17-C16-C11	118.9(2)	C20-C29-C28	120.5(2)

C) Quantum Chemical Calculation

From each solid, a cluster containing the unit cell is selected, taking a central molecule and its surrounding first neighbors. Then, all dimers including the central molecule are investigated. As it has been previously shown,[1,2] dimers can be a good approximation to investigate the intermolecular forces that govern the structure formation even though in some cases larger subclusters (e.g. timers, tetramers) might be needed to capture the full energetics.[3] Furthermore, the sum of the dimer interaction energies are compared to an approximation of the cohesion energy, which is obtained by calculating the full cluster and the full cluster without the central molecule. (See Figures 5 and 6).

For all the DFT functionals the D3BJ correction was included to account for dispersion,[4,5] with exception of M062x, where a ZERO damping was used instead. In order to extract the dispersion component from the DLPNO-CCSD(T) calculations, we used the Local Energy Decomposition (LED) method.[6,7] All the calculations were run with ORCA (version 5.0).[8] Figure 4 depicts the dimer formation energies, defined as: $\Delta E=E_{dimer}-E_{mono1}-E_{mono2}$.

The data in Figure 4 shows that the functionals PBE, PBE0 and TPSS are the ones that yield the best agreement with the DLPNO-CCSD(T) interaction energy. While PBE0 appears to be the best choice for total formation energies, its dispersion correction deviates from the DLPNO-CCSD(T) LED value. In contrast to this, the TPSS dispersion correction exhibits a much better agreement. Table S6 lists the errors of the different DFT functionals and their D3 correction with respect to DLPNO-CCSD(T).

Table S6. Errors in kJ/mol of the DFT-D3 functionals with respect to DLPNO-CCSD(T). Numbers in parenthesis are the corresponding percentage errors (%).

	Top Y		**Side X**	
Functional	Total	Dispersion	Total	Dispersion
B3LYP	-26.23 (22.31)	-24.77 (17.04)	-1.62 (7.92)	-2.13 (9.18)
PBE	8.19 (9.85)	35.62 (41.95)	-0.04 (0.19)	4.40 (26.40)
PBE0	-4.46 (4.66)	30.09 (33.27)	-0.29 (1.53)	3.93 (22.91)
TPSS	-14.03 (13.31)	1.52 (1.27)	-0.99 (4.98)	-0.19 (0.91)
M06-2x	2.48 (2.79)	109.67 (1009.48)	5.91 (45.73)	15.94 (310.88)
BP86	-60.97 (40.03)	-50.92 (29.70)	-2.66 (12.40)	-5.46 (20.59)

To investigate the contributions of the different dimers on the overall structure formation, we used PBE, PBE0 and TPSS in the following. Note that in the following, we drop the '-D3' for simplicity of notation, but all results shown throughout the manuscript include the dispersion correction.

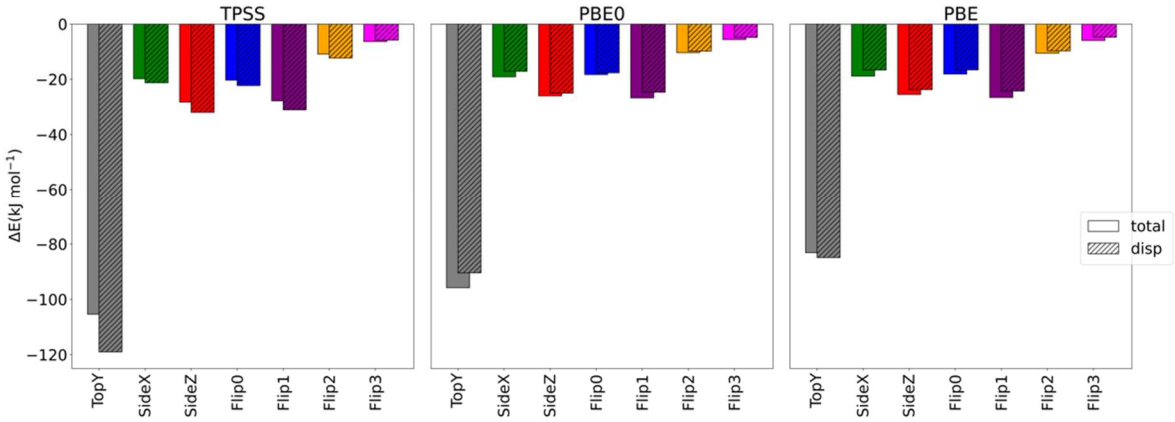

Figure S7. Comparison between the different dimers formation energies at the TPSS (left), PBE0 (middle) and PBE (right) level of theory. The def2-TZVPP basis set was used in each case. Geometries are fixed to the experimental ones.

The results of TPSS, PBE0 and PBE are in good agreement within what can be expected from DFT. With the TPSS functional, which has been shown to be the one to better capture this interaction, we can see how dispersion is consistently stronger that the total interaction across all dimers, overcoming the otherwise repulsive interactions. A detailed analysis of these results (with the PBE0 functional) can be found in the main text.

Table S7 compares the approximation of the cohesion energy, defined as the energy to insert the central molecule into the cluster, with the sum of the formation energies of the dimers. If the dimer approximation is valid, their formation energy should add up to the total cohesion energy. Overall, the difference of the sum of all dimer interactions and the computed cohesion energy approximation is in the range of a few percent. This confirms that the dimer approximation is a fairly good approach to quantify and assess the interactions that govern the crystal structure stability.

Table S7. Comparison of the approximate cohesion energy for the Bi_2Naph_2 cluster and the sum of dimer interaction energies.

	Cohesion (kJ mol^{-1})	**Dimer Sum (kJ mol^{-1})**	**Error (%)**	**Per dimer Error (%)**
TPSS	-396.68	-411.94	3.70	0.31
PBE0	-334.14	-354.04	5.62	0.47
PBE	-371.39	-381.16	2.56	0.21

Figure S10 and Table S8 report, for As, the same analysis carried out for Bi in figure S9 on the dimer formation energies and cohesion energy. Finally, Table S9 lists the formation energies of the optimized dimers, as depicted in Figure 8 in the main text

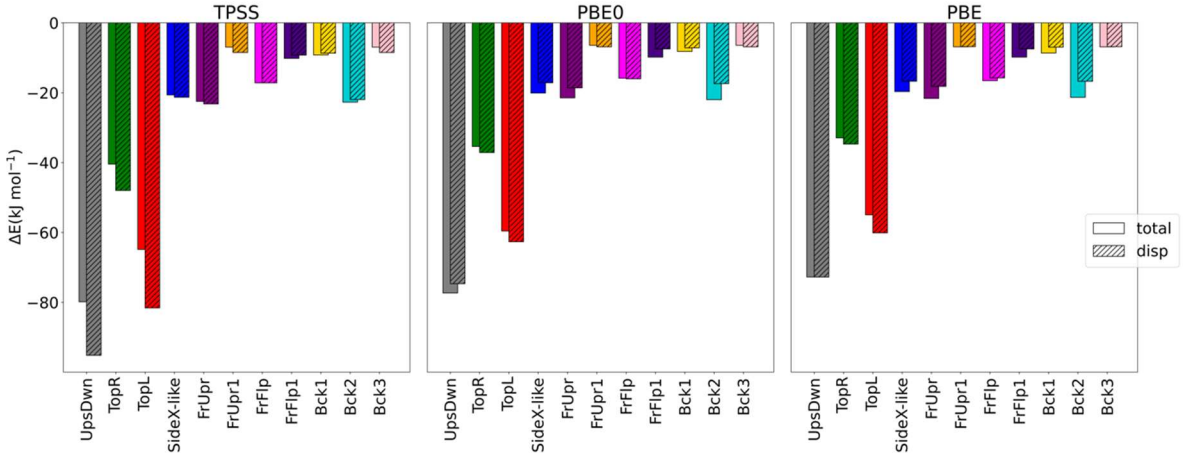

Figure S8. Comparison between the different dimers formation energies from the As structure at the TPSS-D3 (left), PBE0-D3 (middle) and PBE-D3 (right) level of theory. The def2-TZVPP basis set was used in each case. Geometries are fixed to the experimental ones.

Table S8. Comparison of the approximated cohesion energy of the As_2Naph_2 cluster and the dimer sum.

	Cohesion (kJ mol^{-1})	**Dimer Sum (kJ mol^{-1})**	**Error (%)**	**Per dimer Error (%)**
TPSS	-321.04	-344.48	7.30	0.66
PBE0	-305.28	-324.05	6.15	0.56
PBE	-285.92	-313.29	9.57	0.87

Table S9. Formation energies of the optimized dimers depicted in Figure 9 with different pnictogen atoms.

	P		**As**		**Sb**		**Bi**	
(kJ mol^{-1})	ΔE_{tot}	ΔE_{disp}	ΔE_{tot}	ΔE_{disp}	ΔE_{tot}	ΔE_{disp}	ΔE_{tot}	ΔE_{disp}
Top Y	-67.24	-77.52	-74.55	-83.05	-87.15	-92.89	-95.73	-96.04
UpsDwn	-73.61	-76.46	-76.08	-79.64	-78.24	-81.66	-78.39	-82.2
Top L	-58.88	-59.94	-61.7	-63.71	-66.1	-69.86	-70.13	-73.32

IV. References

[1] C. Ganesamoorthy, S. Heimann, S. Hölscher, R. Haack, C. Wölper, G. Jansen and S. Schulz, *Dalton Trans.* 2017, ***46***, 9227.

[2] K. Dzialkowski, A. Gehlhaar, C. Wölper, A. A. Auer and S. Schulz, *Organometallics* 2019, **38**, 2927.

[3] A.-M. Preda, M. Krasowska, L. Wrobel, P. Kitschke, P. C. Andrews, J. G. MacLellan, L. Mertens, M. Korb, T. Rüffer, H. Lang, A. A. Auer and M. Mehring, *Beilstein J. Org. Chem.* 2018, ***14***, 2125.

[4] S. Grimme, J. Antony, S. Ehrlich and H. Krieg, *J. Chem. Phys.* 2010, **132**, 154104.

[5] S. Grimme, S. Ehrlich and L. Goerigk, *J. Comput. Chem.* 2011, **32**, 1456.

[6] W. B. Schneider, G. Bistoni, M. Sparta, M. Saitow, C. Riplinger, A. A. Auer and F. Neese, *J. Chem. Theory Comput.* 2016, **12**, 4778.

[7] G. Bistoni, A. A. Auer and F. Neese, *Chem. Eur. J.* 2017, **23**, 865.

[8] F. Neese, *WIREs Computational Molecular Science* 2018, **8**, e1327.